

# Hindcast of extreme sea states in North Atlantic extratropical storms

Sonia Ponce de León · Carlos Guedes Soares

Received: 26 March 2014 / Accepted: 19 November 2014 / Published online: 18 December 2014  
© Springer-Verlag Berlin Heidelberg 2014

**Abstract** This study examines the variability of freak wave parameters around the eye of northern hemisphere extratropical cyclones. The data was obtained from a hindcast performed with the WAVE Model (WAM) model forced by the wind fields of the Climate Forecast System Reanalysis (CFSR). The hindcast results were validated against the wave buoys and satellite altimetry data showing a good correlation. The variability of different wave parameters was assessed by applying the empirical orthogonal functions (EOF) technique on the hindcast data. From the EOF analysis, it can be concluded that the first empirical orthogonal function (V1) accounts for greater share of variability of significant wave height (Hs), peak period (Tp), directional spreading (SPR) and Benjamin-Feir index (BFI). The share of variance in V1 varies for cyclone and variable: for the 2nd storm and Hs V1 contains 96 % of variance while for the 3rd storm and BFI V1 accounts only for 26 % of variance. The spatial patterns of V1 show that the variables are distributed around the cyclones centres mainly in a lobular fashion.

**Keywords** Wind waves · WAM model · North Atlantic extratropical storms · Extreme sea states · Benjamin-Feir index · Empirical orthogonal functions

---

Responsible Editor: Oyvind Breivik

This article is part of the Topical Collection on the *13th International Workshop on Wave Hindcasting and Forecasting in Banff, Alberta, Canada October 27 - November 1, 2013*

---

S. Ponce de León · C. Guedes Soares (✉)  
Centre for Marine Technology and Engineering (CENTEC), Instituto Superior Técnico, Universidade de Lisboa, Av. Rovisco Pais, 1049-001 Lisbon, Portugal  
e-mail: c.guedes.soares@centec.tecnico.ulisboa.pt

## 1 Introduction

Extreme sea states are often generated by high wind speeds in atmospheric low pressure systems (extratropical storms). The significant wave height of extreme sea states depends on a number of factors such as wind speed, fetch and storm duration.

Changes in storm activity over different time periods have been reported in some studies which cover periods from about 1958 onwards. The storm track activity in the northern hemisphere was studied in Chang and Fu (2002) who found that storm intensities increased by about 30 %. In particular in the Atlantic Ocean, several indications of increased storm intensity have been given by various authors such as Bacon and Carter (1991), Hogben (1994), Kushnir, et al. (1997) and Gulev and Grigorieva (2004).

While storms move and change direction, some of the storm statistics are based on data from a single location not following the storm as discussed in Bernardino et al. (2008). A noticeable shift of the location of the North Atlantic storm tracks was found in McCabe et al. (2001) who showed that storm frequency in midlatitudes decreased during the second half of the twentieth century while an increase was found for the high latitudes north of 60° N. At the same time, storm intensities increased at high latitudes, whereas in midlatitudes they remained nearly constant (Weisse et al. 2005).

On the other hand, Bengtsson and Hodges (2006) pointed out that in some areas, such as over the eastern North Atlantic, there are indications that storms are reactivated. The largest mean intensity is found in the Atlantic Ocean south of Greenland, suggesting an important contribution of the transient eddies to mean flow pressure centres in the northern Atlantic (Icelandic low). However, they also found no indication of any dramatic changes in the number of storms and their intensity either in the extratropics or in the tropics. North Atlantic high occurrence of very extreme sea states region

was already identified in Cardone et al. (2011) based in more than 10 years of satellite altimetry data from the GLOBWAVE database (Ash et al. 2012). Cardone et al. (2011) analysed the wind speed and wave height from seven missions spanning the period August 1991–March 2010. They scanned, filtered and distilled these data using automated and man-machine mix procedures to yield over 5000 basin specific orbit segments with peak  $H_s > 12$  m, which were distilled to a population 120 individual storms in which there was at least one altimeter estimate of  $H_s > 16$  m.

The objectives of the present study are to describe the main features of independent extratropical storms as case studies in the North Atlantic by applying a spectral wave model and using the empirical orthogonal functions (EOF) technique (Hannachi et al. 2007) around the eye of a cyclone. The WAVE Model (WAM) model has already been adopted to study different conditions in the North Atlantic (e.g. Ponce de Leon and Guedes Soares 2005), including some storms (e.g. Ponce de Leon and Guedes 2012) and even in situations where abnormal or rogue waves have occurred (Tamura et al. 2009; Cavaleri et al. 2012).

This work is focused on three case studies that have been identified in Cardone et al. (2011) and Hanafin et al. (2011) with  $H_s$  higher than 9 m based on the wave buoy 62,081 records (latitude  $51^\circ$  N; 251 longitude  $13.36^\circ$  W, B1 in Fig. 1). The threshold of 9 m was considered as minimum value of  $H_s$  for the duration of the extreme storms.

EOF analysis is a widely used method in meteorology and oceanography (Fukuoka 1951; Lorenz 1956; Guedes Soares and Neves 2006; Monahan et al. 2009). However, the application of EOF for modelling  $H_s$  was previously used in few studies such as the work of Lionello and Sanna (2005) for the Mediterranean Sea. Since the waves are generated by winds, this is one of the reasons for use the EOF technique.

The variability of significant wave height ( $H_s$ ), peak period ( $T_p$ ), Benjamin-Feir index (BFI) and directional spreading (SPR) around three powerful extratropical cyclones was assessed by applying the EOF technique on the hindcast data around the eyes of the cyclones of February 2007, February 2011 and February 2013.

The paper is structured as follows: section 2 is devoted to the methods, giving a brief description and configuration of the wave model used. Additionally, section 2 introduces the empirical orthogonal function analysis method. Section 3 gives the common and different features of each extratropical storm. Section 4 deals with the validation of the reanalysis of National Oceanic and Atmospheric Administration (NOAA) and hindcast using records from wave buoys and satellite data; section 5 is devoted to the results. In section 6, the analysis of the EOF is given, and section 7 concludes the work.

## 2 Methods

### 2.1 The WAM model

This work used the version Cy38r1 (ECMWF 2012), which is the latest one of the WAM model (Komen et al. 1994) of the European Centre for Medium-Range Weather Forecasts (ECMWF). The WAM model is formulated in terms of the frequency-direction spectrum  $E(\omega, \theta)$  of the variance of the surface elevation (Janssen and Bidlot 2009). The dissipation source function in this version of WAM has been reformulated in terms of a mean steepness parameter and a mean frequency (Bidlot et al. 2005). The bottom friction dissipation is modelled by the Joint North Sea Wave Project (JONSWAP) formulation (Hasselmann et al. 1973) and the depth-induced breaking is based on the Battjes and Janssen (1979). The wind input follows the Janssen theory (Janssen 1991), and the four nonlinear wave-wave interactions are parameterized by the discrete interaction approximation (DIA).

### 2.2 The reanalysis of NOAA and the bathymetry

The reanalysis were obtained from the Climate Forecast System Reanalysis (CFSR) of NOAA (Saha et al. 2010). The CFSR includes coupling of atmosphere and ocean during the generation of the 6 h guess field, an interactive sea-ice model, and assimilation of satellite radiances. The CFSR global atmosphere resolution is about 38 km with 64 levels. The global ocean is  $0.25^\circ$  at the equator, extending to a global  $0.5^\circ$  beyond the tropics, with 40 levels. The NCEP CFSR hourly time-series products were used with a temporal resolution of 1 h, coverage from January 1979 to December 2010, available at spatial resolution of  $0.31^\circ$ .

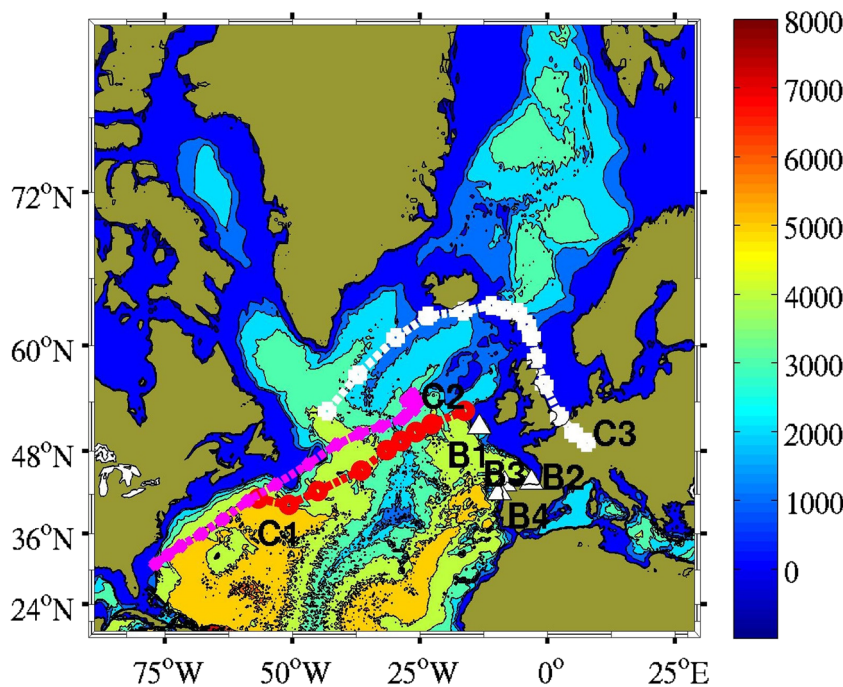
The WAM model configuration covers almost the whole North Atlantic Ocean ( $18^\circ$  N,  $80^\circ$  N,  $90^\circ$  W,  $30^\circ$  E) at a spatial resolution of  $0.25^\circ$  (Fig. 1). The bathymetry grid data were retrieved from the GEODAS NOAA's National Geophysical Data Centre (NGDC), with a resolution of 1 min of degree in latitude and longitude. The bathymetry was linearly interpolated to the  $0.25^\circ$  model grid.

### 2.3 The WAM model configuration

The simulations were performed for the winters of 2007, 2011 and 2013 in which extreme  $H_s$  values have been already observed by satellites (Cardone et al. 2011) and wave buoys. CFSR wind fields were linearly interpolated in space to  $0.25^\circ$  to match with the spatial resolution of the WAM model mesh. The WAM hindcast began at each 15th January, and the temporal resolution was set to one hourly wind input/output time step.

The solution of the energy balance equation was provided for 36 directional bands and 30 frequencies logarithmically

**Fig. 1** The study region, the GEODAS bathymetry grid, the locations of the wave buoys (B1, B2, B3, B4) and WAM outputs. B1—buoy 62081, B2—Bilbao-Vizcaya, B3—Villano-Sizargas, B4—Cabo Silleiro. The extratropical cyclones tracks: C1—February 2007 (red circles dashed line), C2—February 2011 (magenta dashed line), C3—February 2013 (white boxes dashed line)



spaced from the minimum frequency of 0.0350 up to 0.5552 Hz (Table 1). JONSWAP spectrum at every grid point was set as initial condition with the following parameters: Phillips’ parameters 0.18, peak frequency 0.2 Hz, overshoot factor 3.0, left peak width 0.07, right peak width 0.09, wave direction 0°, fetch 30 000 m.

#### 2.4 The extreme wave parameters in the WAM model

From a deterministic set of equations (Zakharov equation and the nonlinear Schrodinger equation) Janssen (2003) proved

**Table 1** WAM model numerical parameters

Parameter	Grid
Integration time step	160 s
Spatial resolution	0.25°(27.8 km)
Number of points (x, y)	(481, 249)
Propagation	Spherical
Frequencies	30
Directional bands	36
Frequency domain	0.0350–0.5552 Hz
Latitudes (°N)	18°;80°
Longitudes (°W)	90°
Longitudes (°E)	30°
Type of model	Deep water
Wind input time step	1 hourly
WAM output time step	1 hourly
NCEP CFSR wind field spatial resolution	0.31°

that these equations admit freak wave-type solutions. He extended the standard theory of four-wave interactions by including effects of nonresonant interactions and derived an expression for the kurtosis in terms of the action density function. Recently comparisons of the predictions of this equation with laboratory measurements showed good agreement (Zhang et al. 2014). The nonlinear four-wave transfer is related with the generation of higher-order cumulants such as the kurtosis ( $C_4$ ). Deviations of the surface elevation pdf from the normal distribution can therefore be expressed in terms of a six-dimensional integral involving the cube of the action spectrum. With  $\eta$  being the surface elevation, the definition of kurtosis is given as:

$$C_4 = \frac{\langle \eta^4 \rangle}{3\langle \eta^2 \rangle^2} - 1 \tag{1}$$

Kurtosis is related to the frequency spectrum  $E(\omega, \theta)$  (Janssen 2003; Janssen and Bidlot 2009) by,

$$C_4 = \frac{4g}{m_0^2} P \int d\omega_1 d\omega_2 d\omega_3 d\theta_1 d\theta_2 d\theta_3 T_{1,2,3,4} \sqrt{\frac{\omega_4}{\omega_1 \omega_2 \omega_3}} \frac{E_1 E_2 E_3}{\Delta\omega} \tag{2}$$

where  $P$  denotes the principal value of the integral and  $\Delta\omega = -\omega_1 + \omega_2 - \omega_3 - \omega_4$ , and  $T_{1,2,3,4}$  is a complicated, homogeneous function of the four wave numbers  $\mathbf{k}_1, \mathbf{k}_2, \mathbf{k}_3, \mathbf{k}_4 = \mathbf{k}_1 + \mathbf{k}_2 - \mathbf{k}_3$ . In addition, the angular frequency  $\omega(\mathbf{k})$  obeys the dispersion relation  $\omega(\mathbf{k}) = g\mathbf{k}$ , with  $\mathbf{k}$  the magnitude of the wavenumber vector  $\mathbf{k}$ .

It was found a fit for the maximum of the kurtosis which follows from the narrow-band limit of the Zakharov equation (Janssen 2003),

$$C_4^{dyn} = \frac{0.031}{\delta_\theta} \times \frac{\pi}{3\sqrt{3}} \text{BFI}^2 \quad (3)$$

where BFI is the Benjamin-Feir index which is given by

$$\text{BFI} = \frac{\sqrt{2\varepsilon}}{\delta_\omega} \quad (4)$$

where  $\varepsilon = k_0 \sqrt{m_0}$  the integral steepness parameter,  $k_0$  is the peak wave number,  $m_0$  the spectral zero moment and  $\delta_\omega$  is the relative width of the frequency spectrum (Janssen 2003). Kurtosis was found to influence the probability of detecting abnormal waves in sea states in the ocean (Cherneva et al. 2011). These waves can occur under normal storm conditions (Guedes Soares et al. 2003; Magnusson and Donelan 2013) or during hurricanes and typhoons (Guedes Soares et al. 2004; Mori 2012).

### 2.5 Empirical orthogonal functions

The method of empirical orthogonal functions (EOF) analysis aims at finding spatial and temporal modes of variation (the EOF's) of a quantity  $q$  that varies in space and time. The identification of the modes is based on how much of the variability of  $q$  they explain. To obtain the EOF's (Monahan et al. 2009) of  $q$  in a given space and time domain,  $n_t$  maps of  $q$  are collected for the period of interest, where each map is a collection of values of  $q$  measured at  $n_p$  locations. The data matrix  $Q(n_p, n_t)$  is then formed by arranging each map into a column so that each row of  $Q$  is the time series of  $q$  at a specific location. The square covariance matrix with dimension  $n_t$  is then formed

$$R = Q^T Q' \quad (5)$$

where  $Q'$  is the anomaly matrix, i.e.  $Q$  with the time average removed at each spatial point. The solution of the eigenvalue problem for  $R$  will return  $n_t$  eigenvalues  $\lambda_i$  and  $n_t$  eigenvectors  $c_i$ . The  $c_i$ 's are called the temporal EOF's of  $q$  and the corresponding eigenvalues  $\lambda_i$ 's give a measure of the variability of  $q$  associated with the mode  $i$ . To obtain the spatial modes  $V_i$ , the  $Q'$  matrix is projected on to the space defined by the  $c_i$ 's:

$$V_i = Q' c_i \quad (6)$$

The original data  $Q'$  for time  $j$  then may be recovered by

$$Q'_j = \sum_{i=1}^{n_t} V_i c_{ij} \quad (7)$$

where  $c_{ij}$  is the value of  $c_i$  at time  $j$ . If a truncated representation of  $Q$  is sought, then the sum in Eq. (7) may proceed only up to a certain  $p < n_t$ .

### 2.6 Representation of spatial maps in the polar grid

The hindcast fields and the EOF's for the wave parameters were linearly interpolated to a latitude-longitude grid centred at the cyclone's centre position. National Snow and Ice Data Center (NSIDC) database of northern hemisphere cyclone location and characteristics (Serreze 2009) was used to obtain the location of the 2007 cyclone centre. This data set contains half a century of daily extratropical cyclone statistics, such as centre location and sea level pressure (SLP) with a temporal coverage from 1958 up to 2008. The tracks of the storm centres for the 2011 and 2013 storms were obtained from the NOAA Global Forecast System (GFS) analysis data which is a weather forecast model of the National Centers for Environmental Prediction (NCEP) (Environmental Modeling Center 2003).

## 3 Extratropical storms

In this section, common and different features were compiled taking into account the duration, intensity and the region of the generation. This information was obtained mainly from the synoptic charts from United Kingdom Meteorological Office (UKMO).

The storms were called C1 (8–10 February 2007), C2 (12–17 February 2011) and C3 (4–6 February 2013). C1 and C2 were previously described in Cardone et al. (2011) and Hanafin et al. (2011), respectively.

Table 2 summarizes the main characteristics of the North Atlantic storms. At B1, the maximum recorded value of Hs was 13.80 m. This extreme value was the highest observed having occurred in the second of the two intense extratropical cyclones of February 2007. These two storms were highlighted in the Mariners Weather Log review of North Atlantic Ocean storms (Bancroft 2007); wind speeds equivalent to category 3 hurricane were measured by QuikScat. The altimetry Hs peak value of 20.24 m on 10 February at 11:08 UTC was estimated from GFO satellite Ku-band altimeter at a latitude of 48.14° N and longitude of 32.65° W (Cardone et al. 2011).

The threshold of 9 m was considered as minimum value of Hs for extreme waves at location P1; in accordance with this threshold, the duration of each storm was estimated.

The North Atlantic storm durations usually vary from 14 up to 144 h (6 days) according to Almeida et al. (2011) who examined the period from 1952 up to 2009. In the present study, the duration of the storms varied at B1, ranging from 40

**Table 2** Winter extratropical storms (case studies) features and the associated freak wave parameters computed with the WAM model at location B1 (see Fig. 1). WAM Hs values are given in parenthesis. The deepening rate was calculated according to the low pressures surface analysis charts (UKMO)

Parameters	8–10 February 2007 (C1)	12–17 February 2011 (C2)	4–6 February 2013 (C3)
Duration	42 h	120 h	40 h
Minimum pressure centre (mb)	952 (9 Feb. 06 UTC)	950 (14 Feb. 00 UTC)	953 (3 Feb. 18UTC)
Maximum deepening rate (mb/h)	36 mb/24 h=1.50	34 mb/24 h=1.42	38 mb/24 h=1.58
Maximum Hs (m)	13.80 (14.24)	11.20 (13.06)	(13.18)
WAM directional spreading	0.32°	0.39°	0.41°
AI=Hmax/Hs index	1.94	1.99	1.95
BFI index	0.38	0.77	0.25
Kurtosis	3.07	3.13	3.04

up to 120 h (Table 2). C1 and C3 have a similar duration (40–42 h) and the longest was C2 (120 h) (Table 2).

The three extreme storms have in common their genesis. They followed an explosive cyclogenesis and experienced similar deepening rates ranging from 1.42 up to 1.6 mb/h (Table 2). However, C1 and C3, having a similar duration, had different deepening rates. This rate was higher (1.6) for C3 (Table 2). The lowest pressure was recorded during C2 (950 mb).

Sanders and Gyakum (1980) characterized a rapidly deepening of an extratropical cyclone as one in which the central pressure dropped 1 mb/h for 24 h. They observed a tendency for the more explosive storms (called “bombs”) to occur preferentially in the Atlantic Basin where gradients are strongest in longitudes west of 40° W and between 35 and 50° N.

Storm C3, which had the highest deepening rate, was observed to the northeast of Nova Scotia at the 2nd of February 2013 at 12 UTC around the 45° latitude north. This system travelled across the North Atlantic moving to the northeast. All the analysed storms which were generated on the west side of the Atlantic Ocean were mainly observed between the 40 and 50° N latitudes; however, C3 rapidly moved northeastwards reaching the 64° N latitude around which it remained almost stationary near the Faroe Islands. A deep area of low pressure was observed from the UKMO synoptic charts (not shown) tracking to the north of Scotland around 3–5 February 2013, generating very large waves. The main difference between the three storms was that C3 reached higher latitudes than these extreme events usually do as reported in Sanders and Gyakum (1980).

The storms analysed are of similar type, mostly generated over the southern region of North America or in the area situated to the south or southeast of Newfoundland. This kind of cyclones was already classified in Nesterov and Lukin (2012). In their work, these cyclones were classified as “second type” with a 20 % of frequency of occurrence for the 2002–2011 period.

### 3.1 Storm parameters along the tracks

The evolution along the tracks of the main parameters that describe C1, C2 and C3 was represented in Fig. 2. It can be seen that at  $t=0$  the direction of propagation (top panel) was similar for C1 and C2 (NE sector). These two storms maintained their course due northeast during all the tracking period. C3 had a different track, starting to be tracked when heading northeast close to 50°, but then gradually turning southeast during the tracking period. Note that C3 exhibited the largest northward excursion of all three storms.

The atmospheric pressure had almost the same behaviour for C1 and C3 during the first 48 h. It is necessary to point out that the lowest pressure was observed for C3 during this whole period. At the same time, the highest pressure was observed during almost the whole period for C2 which reached the minimum of 950 hPa at the end of the period (bottom panel).

The highest propagation velocity values were found for C1 (122 km/h) at 12 UTC. The velocity for C1 and C3 had in average the same behaviour which decreased with time. However, for C2, the velocity was constantly increasing from  $t=0$  up to 36 h when it started to decrease.

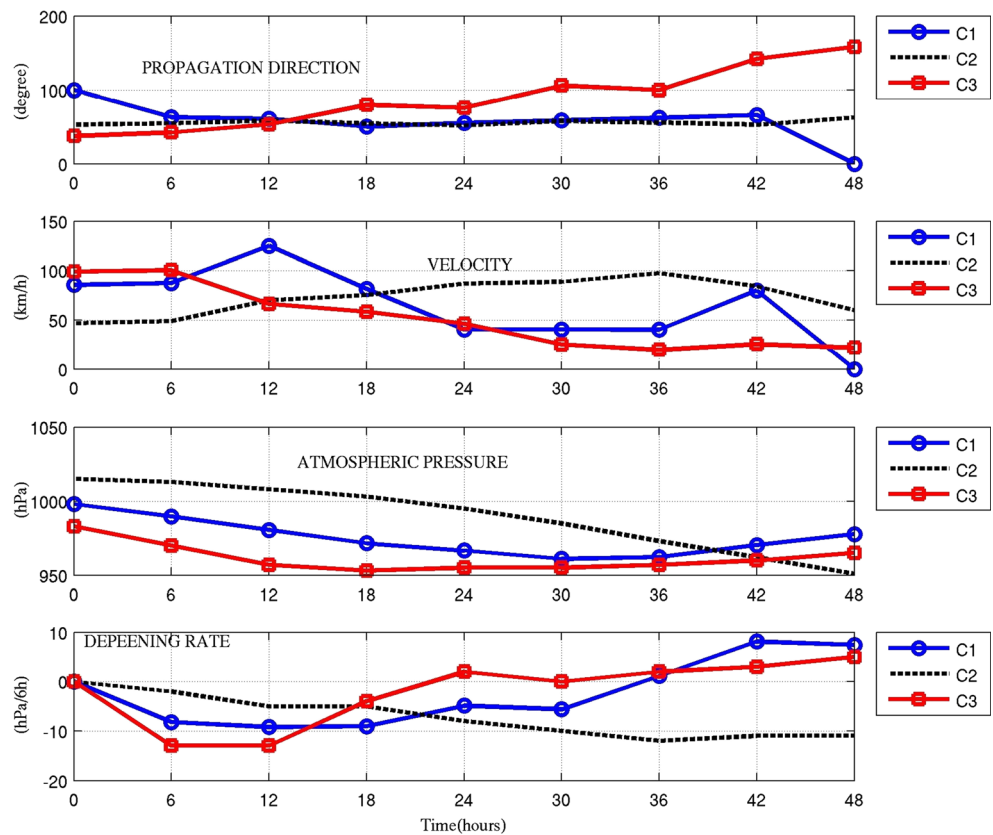
The lowest values of the deepening rate (bottom panel) were reached by C1 and C3 around 6–12 UTC. The lowest deepening rate was observed for C3 during the first 12 h of the tracks. C1 and C3 have a similar increasing behaviour from 12 UTC, a time from which the deepening rate started to increase up to the end. However, C2 had a constant tendency rate of deepening to decreasing along this whole period.

## 4 Validation of the wind forcing and wave hindcast

### 4.1 Wave records

The wave hindcast was validated against four moored wave buoys data (Fig. 1) from two main wave buoys networks: three wave buoys of Puertos del Estado of Spain (Bilbao

**Fig. 2** Evolution along the tracks of C1, C2 and C3 propagation direction (*top panel*), propagation velocity (*second panel*), atmospheric pressure (*third panel*) and deepening rate (*bottom panel*)



Vizcaya, Cabo Silleiro and Villano-Sisargaz) and one from UKMO (62081). All of them are moored in deep waters, and their locations are represented in Fig. 1.

## 4.2 Satellite altimetry data

### 4.2.1 ASCAT

The CFSR reanalysis wind speed was validated against the Advanced Scatterometer (ASCAT) MetOp (Meteorological Operational) satellite observations (Verhoef and Stoffelen 2012). In this study, the wind speed at 10 m height from the level 2 12.5 km Ocean Surface Wind Vectors product was used.

### 4.2.2 JASON2

The WAM hindcast was verified against satellite records. WAM Hs was compared against the GLOBWAVE L2P data (Ash et al. 2012). The GLOBWAVE data employed appropriate quality control and calibration of the data streams from the various missions as described in Queffeuou and Croize-Fillon (2012). WAM model results were interpolated linearly to the position and time of the satellite observations. Details about

JASON2 can be found in the earth observation handbook (2012).

## 5 Results

In this study, the scatter index (SI) was defined as the standard deviation of the predicted data with respect to the best-fit line in a least-squares sense, divided by the mean observations, and the bias was defined as the difference between the mean observation and the mean prediction.

The comparison of the reanalysis of NOAA against the ASCAT observations shows a good agreement between the CFSR and wind speed records. The left panel of Fig. 3 shows a high correlation coefficient (0.96) and slope (0.97) and low scatter index (0.13) and bias (0.31).

Satellite data have the advantage of a great coverage over extended distances around the North Atlantic Ocean and the WAM hindcast have been validated against the altimetry data measurements from JASON2 (Fig. 3, right panel). From the scatter plots for the Hs between WAM and satellite data (Fig. 2), a low scatter index (0.19), a high correlation coefficient (0.93) and a slope of around 0.9 were obtained. Besides, the hindcast was compared against an orbit segment (JASON2) during the extreme sea state conditions of 14

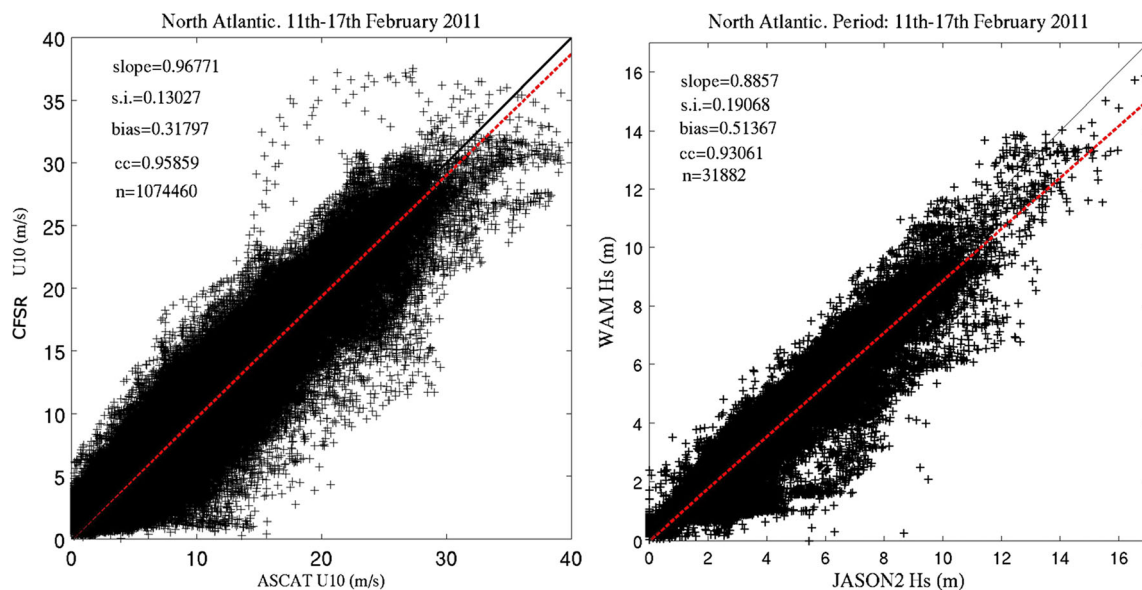


**Fig. 3** Scatter plot for the wind speed (U10) after the collocation between ASCAT data against the CFSR reanalysis (*left*) and scatter plot for the Hs (m) after the collocation between JASON2 data and WAM for a week of February 2011

February 2011 at 00 UTC, from which it can be observed an almost a perfect agreement between the Hs from JASON2 records and the WAM values. Extreme values higher than 15 m can be observed (Fig. 3 (right panel) and Fig. 4).

In addition, the wave hindcast was compared against wave buoys described in section 4. C2, which took place in February 2011, was selected for the validation, showing a good agreement between the WAM values and wave records (Fig. 5). The correlation coefficients were in the range of 0.86–0.9 and low scatter indexes were obtained (0.16–0.19). In general, WAM overestimated the observations for locations B1 (−0.55), B3 (−0.17) and B4 (−0.22) with the obtained

negative biases. At B2, however, the bias obtained was positive (0.36).

This particular extreme event was widely described in Hanafin et al. (2011) using different satellite missions and segments. This system was the last of four deep lows with hurricane-force winds that developed in close succession over the northern Atlantic. On 13 February, C2 was located south of Newfoundland according to synoptic analysis charts of the NOAA Prediction Center.

On 14 February at 00 UTC, C2 had moved to the northeast at a speed of 23.6 m/s and had rapidly intensified by 34 hPa in 24 h. The CFSR wind field for 14 February at 00 UTC shows wind speed of about 35 m/s (Fig. 6). Hurricane-force winds of about 44 m/s were observed by different satellite altimeters. In addition, Bancroft (2011, issue of MWL) reported that JASON2 altimetry data on the 14th at 11 UTC observed 20.1 m of Hs.

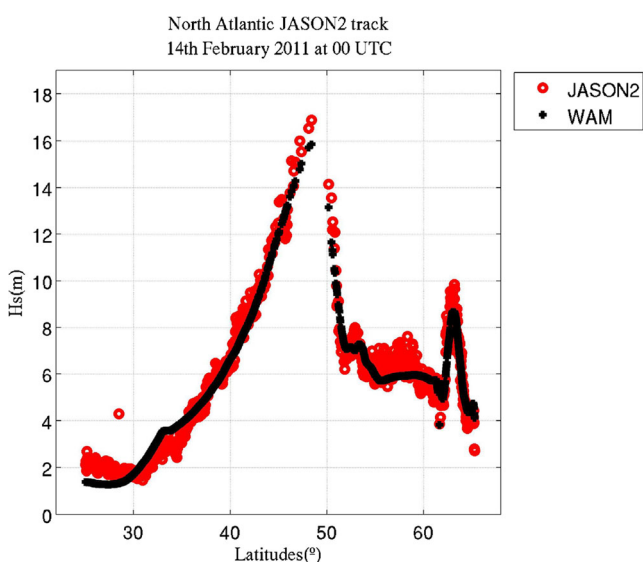


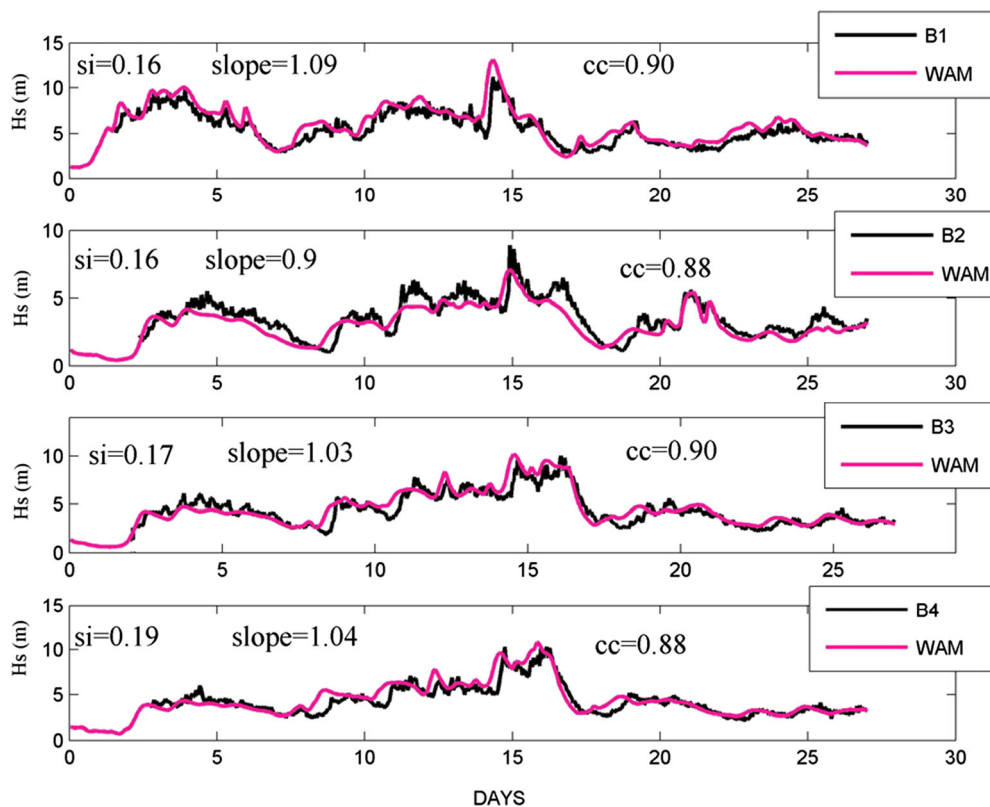
**Fig. 4** Comparison of the WAM Hs against JASON2 Hs measured data along an orbit segment in an extreme sea state condition

### 5.1 WAM extreme wave parameters

Waves are referred to as abnormal or rogue if they exceed 2.0–2.2 times the significant wave height (Guedes Soares et al. 2003; Kharif and Pelinovsky 2003). From Table 2, it can be seen that the highest Hs was obtained during the C1 for which the abnormality index (AI=Hmax/Hs) and the directional spreading were the lower with values of 1.94 and 0.32°, respectively.

For the largest storm duration (C2), the computed abnormal wave parameters resulted the largest too (Table 2, abnormality index=1.99, BFI=0.77, kurtosis=3.13). The freak wave’s parameters for the C1 and C2 were similar (AI=1.94 and 1.95, BFI=0.38 and 0.2, kurtosis 3.07 and 3.04). This can

**Fig. 5** Validation of the WAM hindcast using the wave buoys. *Top panel—B1, second panel—B2, third panel—B3, bottom panel—B4* (see Fig. 1) for the period of 2–28 February 2011

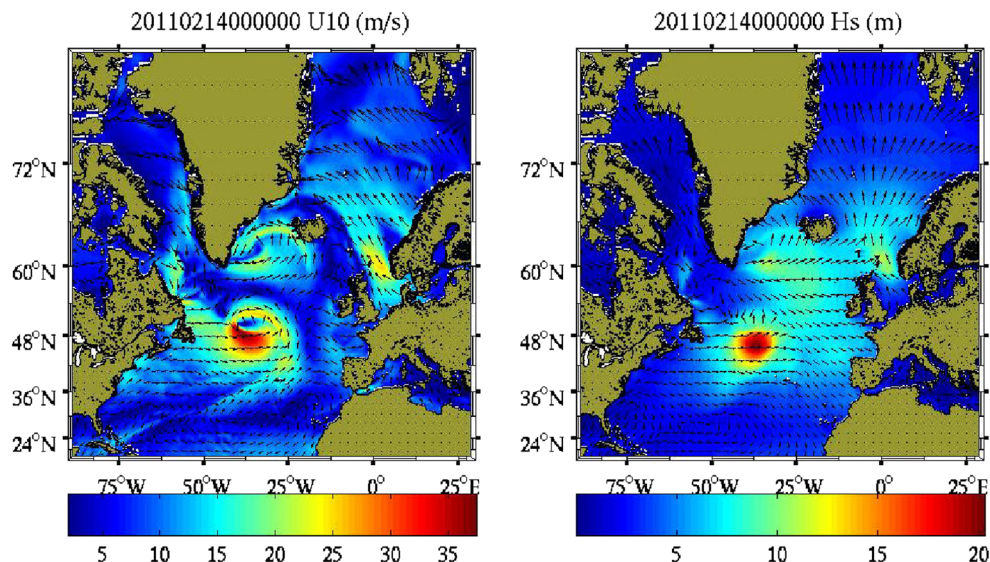


be explained with the fact that they had almost the same duration (40–42 h). However, the largest Hs obtained (13.8 m from records and 14.24 m from WAM) show low BFI of 0.38 and the lowest directional spreading ( $0.32^\circ$ ).

The WAM Hs spatial distributions at the apex of the chosen extratropical storms C1, C2 and C3 are displayed in Fig. 7. Two maxima of Hs (approximately 18 m) can be seen (left panel for the storm of February 2007. Locally nearby B1,

lower values of Hs (14 m) can be observed, and the wave direction propagation is mainly from the west (10th at 05 UTC). In the case of the February 2011 storm at the 15th at 07 UTC (middle panel), different pattern of the Hs maxima values (higher than 14 m) can be seen. The waves generated under this storm conditions were mainly propagating from the west and southwest, reaching the British Islands and the south of European continent. The extratropical storm of the 5

**Fig. 6** The extratropical storm C2 from the CFSR reanalysis of NOAA wind field (*left*) and WAM Hs map (*right*) for 14 February 2011 at 00 UTC





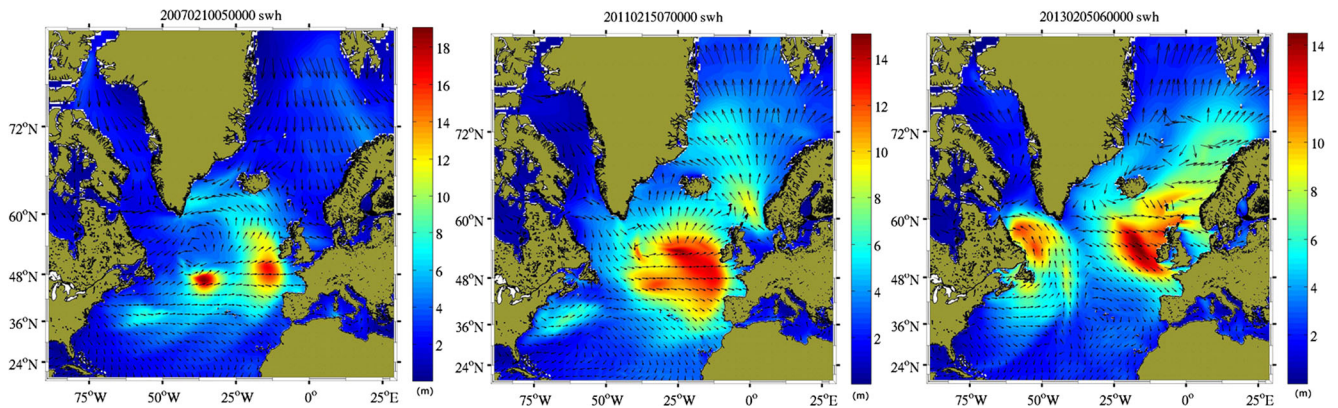


**Fig. 7** WAM significant wave height for the extratropical storms of 10 February 2007 at 05 UTC (*left*), 15 February 2011 at 07 UTC (*middle*) and 5 February 2013 at 06 UTC (*right*)

February 2013 at 06 UTC shows maxima values of  $H_s$  of about 14 m, and the wave main direction propagation was from the NW (*right panel*).

BFI and kurtosis are significantly large mainly in the fourth quadrant, as can be seen from the spatial distribution (*Fig. 8*) and as was before reported in Mori (2012) and Ponce de León and Guedes (2014). In these regions, the probability of occurrence of abnormal waves is high. However, locally at B1, the freak wave parameters are not especially high (*Table 2*). High BFI implies an enhancement of the nonlinearities and a high C4 means a high deviation of the distribution of the maximum wave height from the Rayleigh distribution (Mori and Janssen 2006; Janssen 2003).

The BFI spatial distribution (*Fig. 8*) shows that the highest values of BFI (1.5) were obtained during the storm of February 2007 (C1) which were mainly located to the south-west of the British Islands. These values can be explained in association with the  $H_s$  maximum of *Fig. 7*, in the vicinity of location B1. In the case of the storm of 2011 (C2), the BFI was around 0.75 at the same area with a small strip of higher values of BFI (around 1.5).

In the case of the C3 (of 2013), the maxima values of BFI are observed to the west side of the North Atlantic despite the

fact that  $H_s$  highest values are located (*Fig. 7*) to the SW of British Islands. This means that  $H_s$  values higher than 14 m do not necessary means a high probability of occurrence of a freak wave in this region.

### 6 Analysis of empirical orthogonal functions

The EOF analysis allows identifying the principal modes of variability of the system under consideration. Most of the variability is described by the first EOFs which account for the highest values of the total variability for the different variables (*Tables 3 and 4 and Fig. 9*). The highest variance content of any single mode was obtained for the  $H_s$  variable for C2 (96 %). For this variable, the next stronger variable 1st mode ( $\lambda_1$ ) is that of C1 and the weakest  $\lambda_1$  is that of C3. For the 2nd mode ( $\lambda_2$ ), the opposite occurs and the stronger  $\lambda_2$  occurs for C3 and the weakest  $\lambda_2$  for C2. For the peak period ( $T_p$ ) the strongest  $\lambda_1$  is that of C1, followed by cyclones 2 and 3 while for  $\lambda_2$ , the strongest is that of C3 while the  $\lambda_2$  of cyclones 1 and 2 exhibit similar variances. For the BFI, the strongest  $\lambda_1$  is that of C1, followed by cyclones 2 and 3,

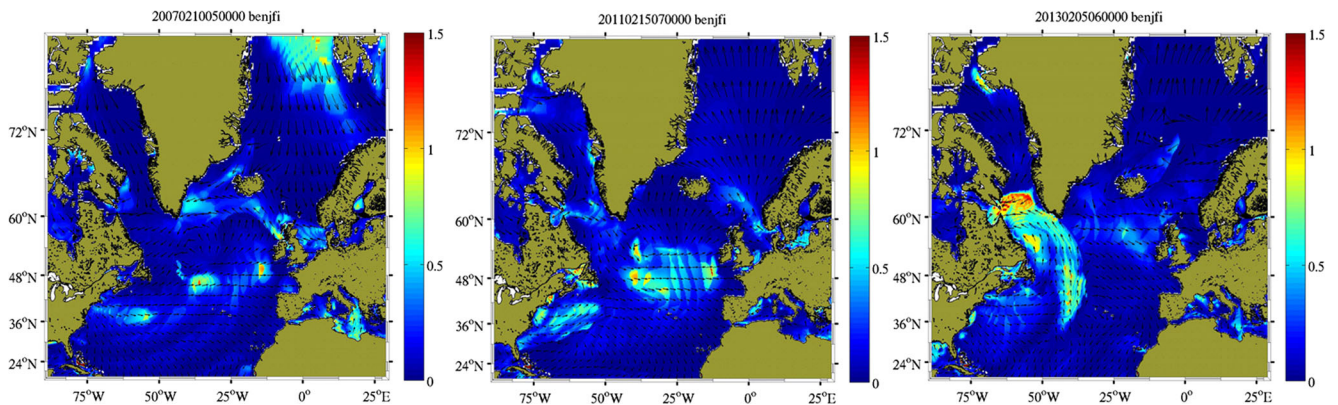


**Fig. 8** BFI for the extratropical storms of 10 February 2007 at 05 UTC (*left*), 15 February 2011 at 07 UTC (*middle*) and 5 February 2013 at 06 UTC (*right*)

**Table 3** Percentage of variance by the first three EOFs of Hs, V1,V2,V3-First, second and third empirical orthogonal function, respectively

EOFs	C1	C2	C3
V1 (%)	83.4	95.8	69.7
V2 (%)	9.4	2.7	14.9
V3 (%)	4.2	0.4	5.6

**Table 4** Percentage of variance by the first EOF of Tp, BFI, Hs and directional spreading

	C1	C2	C3
Hs (%)	83	96	70
Tp (%)	95	86	54
BFI (%)	86	46	26
SPR (%)	57	62	51

whose  $\lambda_1$  have a much lower variance. The weakest  $\lambda_2$  occurs for C1 and for cyclones 2 and 3  $\lambda_2$  has lower variance than  $\lambda_1$ ; although for these two storms, the difference between  $\lambda_1$  and  $\lambda_2$  is lower than for C1 (Fig. 9). For the directional spreading, the mode strengths are similar for all storms.

The first spatial EOF (V1) is depicted in Fig. 10 for the Hs, Tp, directional spreading and BFI and for the three cyclones. The V1 for the Hs is similar for all three storms with the peak intensity (in absolute value) located in the 3rd and 4th quadrants. Remarkably, for C3, the V1 is negative. In Fig. 11 (top panel), the associated temporal mode for the C3 Hs V1 is shown. This mode is slightly positive at first but becomes

negative, indicating a positive contribution of the V1 to the Hs variability of C3. The Tp V1 (Fig. 10, 2nd row) is significantly different for the three storms. For C1, the V1 is positive with two lobes of low intensity aligned with the bisector of the 1st and 3rd quadrants. This spatial mode is especially dominant and shows a constant slightly negative temporal evolution until 48 h into the tracking period where it becomes positive and largely determines the distribution of Tp around the cyclone’s centre. The lobe located in the 1st quadrant coincides with the least intense region of the Hs V1 for C1. Lobe structures are also present in the Tp V1 for cyclones 2 and 3 but are not as clear as for C1 and are populated by small scale spatial patterns. For the directional spreading, the V1 for all three cyclones show a clear lobe structure dividing the mode in low and high intensity areas. C1 has a concentrated high intensity region in the 2nd quadrant while the lower intensity regions are spread out across the 1st, 3rd and 4th quadrants. This mode evolves constantly through the tracking period. The low directional spreading variability associated with this mode occurs in the same region of high Hs variability in this variable’s V1. For C2, there is a similar situation where the high (positive) intensity is located approximately in the same region, and the low (negative) intensity is distributed along a larger area, mainly in the 4th quadrant. This V1 is negative at the first tracking time step but becomes close to zero in the subsequent tracking dates. For C3, the directional spreading V1 presents mostly positive values with maximum intensity in the 2nd and 3rd quadrants. This mode has a time evolution similar to that of C1. The BFI V1 for all cyclones divides the region around the cyclone centre in positive and negative zones. For C1, the negative region is located mainly in the

**Fig. 9** Distribution of variance in the first ten EOFs for the Hs, Tp, BFI and directional spreading around the eye of each cyclone

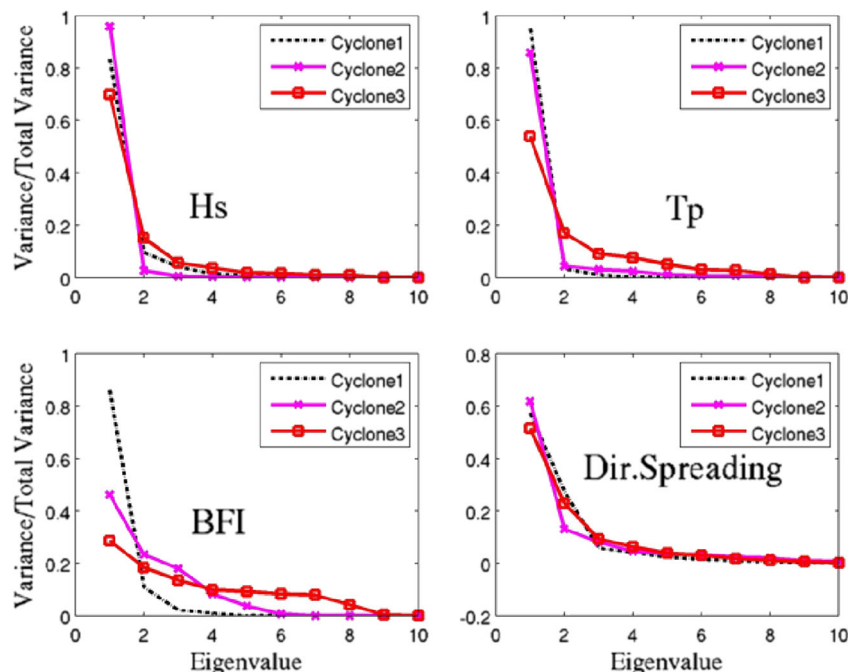
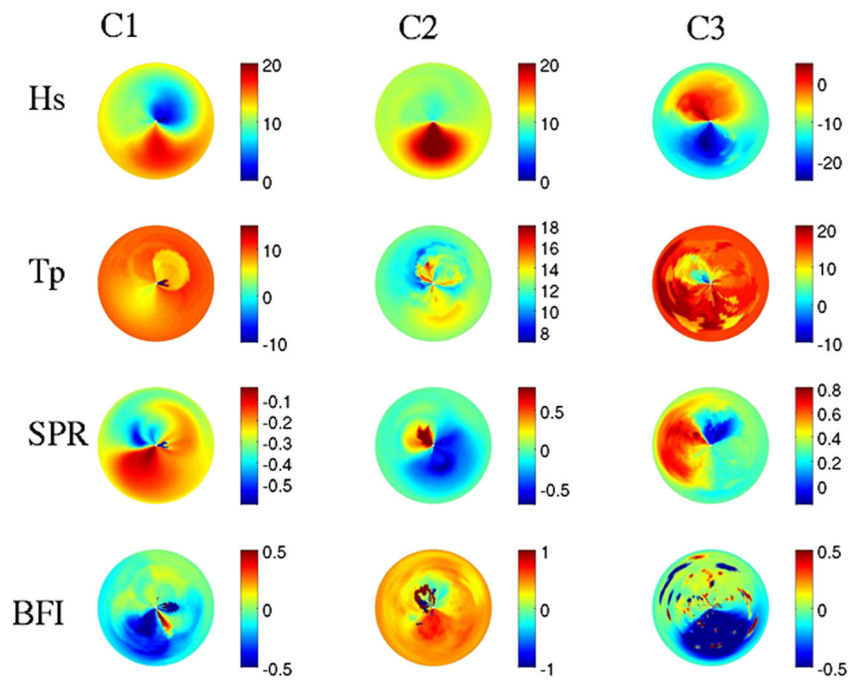


**Fig. 10** V1 for the Hs, Tp, directional spreading (SPR) and BFI around the eyes of the three studied extratropical cyclones (C1, C2, C3)



3rd quadrant coincident with the low intensity region of the directional spreading V1. For C2, this negative region roughly coincides with positive directional spreading. For C3, such relationship is not appreciable in the directional spreading and BFI V1 maps. Furthermore, this last V1 presents small scale patches of high positive/negative values superimposed on the

large scale pattern that are most likely due to land areas occupied by the 500 km to the centre circle used to compute the polar distribution of variables around the cyclones centre.

The observed differences allow to explain the EOF spatial distribution (Fig. 10) because different stages were presented along the tracks C1, C2 and C3. The data available only

**Fig. 11** Amplitudes of the first temporal EOF for three cyclones for Hs (top panel), Tp (2nd panel), BFI (3rd panel), directional spreading (4th panel). Blue circles line—cyclone 1, dashed black line—cyclone 2, red square line—cyclone 3

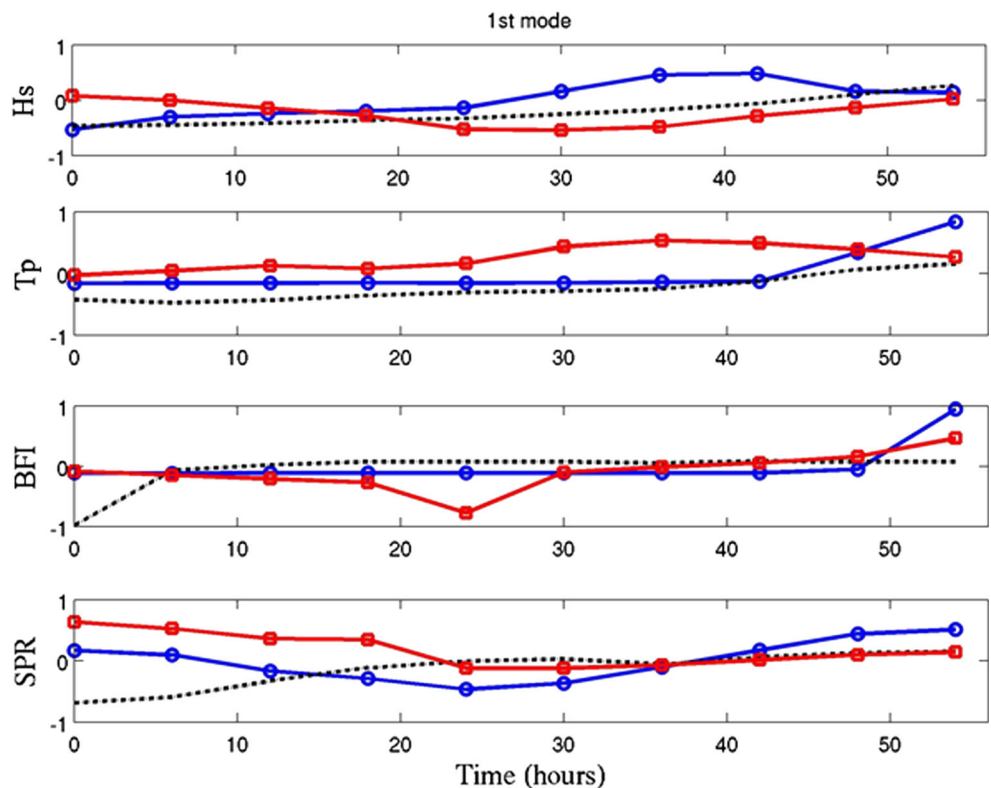
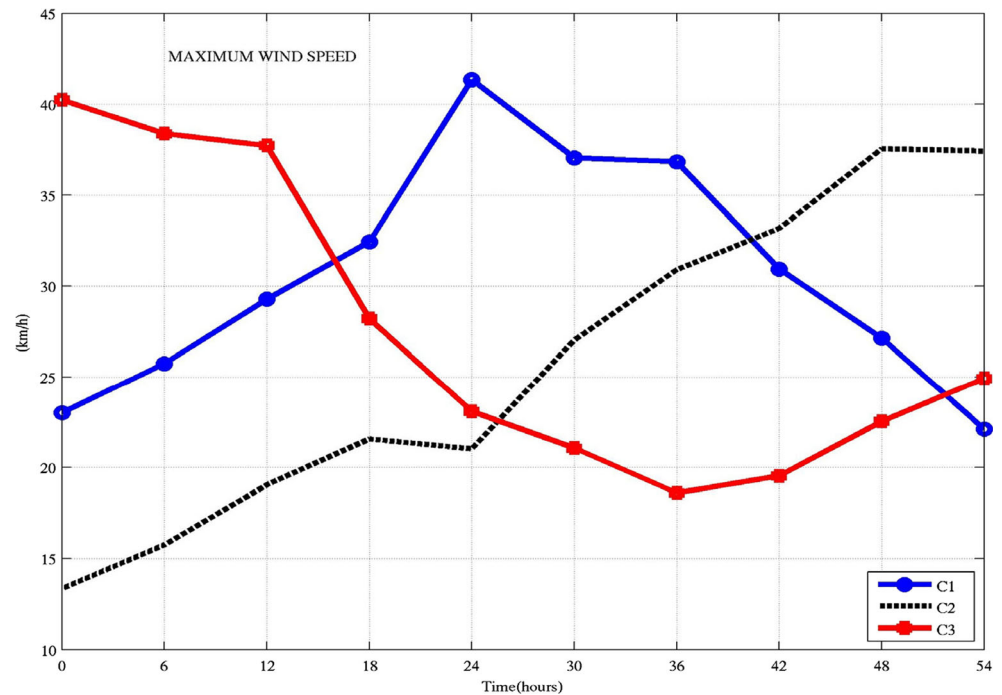


**Fig. 12** Evolution of the maximum wind velocity (km/h) along the tracks for C1, C2 and C3



allows identifying the evolution of the storms with respect to the pressure at the storm's centre. During the tracking period, C1 and C3 go through a pressure minimum at 30 and 18 h, respectively, while C2 continually deepens throughout the tracking period (Fig. 2). One can assume, however, that they are in a development phase (Hart 2003) as the tracking commences since their intensification is still occurring during tracking.

The evolution of the first temporal EOF for the Hs (Fig. 11) follows the evolution of the maximum wind speed (Fig. 12). For C1, an increase of the maximum wind was verified and after that a decrease. The same behaviour was observed for the 1st EOF for Hs. However, for C3, a decrease of the maximum wind speed was verified and a slightly increase at the end of the track. This can explain the “strange” spatial pattern of C3 (Fig. 10). The same behaviour was observed for the 1st EOF for Hs. For C2, both variables increased during the tracking period.

## 7 Conclusions

In this research, the dominant patterns of variation of extratropical cyclones were determined by empirical orthogonal function (EOF) models. From the EOF analysis, it can be concluded that most of the Hs variability is described by the first EOF, which accounts for 83.4, 95.8 and 69.7 % for C1, C2 and C3, respectively. The spatial pattern of the Hs spatial mode indicates a clear difference between the forward part of the cyclone (1st and 2nd quadrants) and the trailing region of the cyclone (3rd and 4th quadrants).

Locally at B1 (not located in the path of the storms), the freak wave parameters are not especially high, ranging from 0.25 up to 0.77 for the three storms analysed (Table 2).

From the obtained results, it can be inferred that the duration of the storms is an important feature for the abnormal wave parameters. The highest values of the abnormality index, BFI and Kurtosis were obtained for the largest C2 (120 h).

**Acknowledgments** Tracks of the 2011 and 2013 storms were kindly made available by Guang Ping of EMC/NCEP. This work has been performed within the project CLIBECO—present and future marine climate in the Iberian coast, funded by the Portuguese Foundation for Science and Technology (FCT—Fundação Portuguesa para a Ciência e a Tecnologia) under contract n.º: EXPL/AAG-MAA/1001/2013. The first author has been funded by Fundação para a Ciência e Tecnologia (Portuguese Foundation for Science and Technology) under postdoctoral grant SFRH/BPD/84358/2012.

## References

- Almeida LP, Ferreira O, Vousdoukas MI, Dodet G (2011) Historical variation and trends in storminess along the Portuguese south coast. *Nat Hazards Earth Syst Sci* 11:2407–2417
- Ash E, Busswell G, Pinnock S (2012) DUE Globwave wave data handbook, Logica, UK Ltd. 74 pp
- Bacon S, Carter DJT (1991) Wave climate changes in the North Atlantic and North Sea. *Int J Climatol* 11:545–558
- Bancroft GP (2007) Marine weather review—North Atlantic area January through April 2007. *Mariners Weather Log* 51, 38–53
- Bancroft GP (2011) Marine weather review—North Atlantic area January through June 2011. *Mariners weather log* 55 number 3, 15–21

- Battjes JA, Janssen JPFM (1979) Energy loss and set-up due to breaking of random waves. In Proc. 16th Int. Conf. Coastal Engineering, 569–587, Hamburg Germany
- Bengtsson L, Hodges KI (2006) Storm tracks and climate change. *J Clim* 19:3518–3543
- Bernardino M, Boukhanovsky A, Guedes Soares C (2008) Alternative approaches to storm statistics in the ocean. Proceedings of the 27th International Conference on Offshore Mechanics and Arctic Engineering (OMAE 2008), Estoril, Portugal. New York, USA: ASME paper OMAE2008-58053
- Bidlot J, Janssen PAEM, Abdalla S (2005) A revised formulation for ocean wave dissipation in CY29R1. Memorandum Research Department, ECMWF, April 7, 2005 File: R60.9/JB/0516
- Cardone VJ, Cox AT, Morrone MA, Swail VR (2011) Global distribution and associated synoptic climatology of very extreme sea states (VESS). Proceedings 12th International workshop on wave hindcasting and forecasting, Hawaii, October 31–November 4, 2011
- Cavaleri L, Bertotti L, Torrisi L, Bitner-Gregersen E, Serio M, Onorato M (2012) Rogue waves in crossing seas: the Louis Majesty accident. *J Geophys Res* 117:C00J10. doi:10.1029/2012JC007923
- Chang EKM, Fu Y (2002) Interdecadal variations in northern hemisphere winter storm track intensity. *J Clim* 15:642–658
- Cherneva Z, Guedes Soares C, Petrova PG (2011) Distribution of wave height maxima in storm sea states. *J Offshore Mech Arctic Eng* 133(4):041601–1–041601–5
- ECMWF (2012) Wave model. Part VII: IFS documentation – Cy38r1. Operational implementation, part VII: ECMWF wave model, pp. 79
- Environmental Modeling Center (2003) The GFS atmospheric model. NCEP office note 442, global climate and weather modeling branch, EMC, Camp Springs, Maryland
- Fukuoka A (1951) A study of 10-day forecast (a synthetic report). *Geophys Mag* 22:177–218, Tokyo
- Guedes Soares C, Neves S (2006) Modelling tidal current profiles by means of empirical orthogonal functions. *J Offshore Mech Arctic Eng* 128(3):184–190
- Guedes Soares C, Chemeva Z, Antao E (2003) Characteristics of abnormal waves in North Sea storm sea states. *Appl Ocean Res* 25(6): 337–344
- Guedes Soares C, Chemeva Z, Antao E (2004) Abnormal waves during hurricane Camille. *J Geophys Res* 109:1–7. doi:10.1029/2003JC002244, ISSN: C08008
- Gulev SK, Grigorjeva V (2004) Last century changes in ocean wind wave height from global visual wave data. *Geophys Res Lett* 31:L24302. doi:10.1029/2004GL021040
- Hanafin JA, Quilfen Y, Ardhuin F, Sienkiewicz J, Queffeuilou P, Obrebski M, Chapron B, Reul N, Collard F, Corman D, de Azevedo EB, Vandemark D, Stutzmann E (2011) Phenomenal sea states and swell from a North Atlantic storm in February 2011: a comprehensive analysis. *Bull Am Meteorol* 93(12):1825–1832
- Hannachi A, Jolliffe IT, Stephenson DB (2007) Empirical orthogonal functions and related techniques in atmospheric science: a review. *Int J Climatol* 27:1119–1152
- Hart RE (2003) A cyclone phase space derived from thermal wind and thermal asymmetry. *Mon Weather Rev* 131:585–616
- Hasselmann K, Barnett TP, Bouws E, Carlson H, Cartwright DE, Enke K, Ewing JA, Gienapp H, Hasselmann DE, Kruseman P, Meerburg A, Müller P, Olbers DJ, Richter K, Sell W, Walden H (1973) Measurements of wind-wave growth and swell decay during the Joint North Sea Wave Project (JONSWAP). *Dtsch. Hydrogr. Z. Suppl. A* 8 (12), 95 pp
- Hogben N (1994) Increases in wave heights over the North Atlantic: a review of the evidence and some implications for the naval architect. *Trans. RINA, V* Vol.137, Part A, pp. 93–115
- Janssen PAEM (1991) Quasi-linear theory of wind-wave generation applied to wave forecasting. *J Phys Oceanogr* 21:1631–1642
- Janssen PAEM (2003) Nonlinear four-wave interactions and freak waves. *J Phys Oceanogr* 33(4):863–884
- Janssen PAEM, Bidlot JR, (2009) On the extension of the freak wave warning system and its verification. Issue 588 of ECMWF technical memorandum, 42 pages
- Kharif C, Pelinovsky E (2003) Physical mechanisms of the rogue wave phenomenon. *Eur J Mech B Fluids* 22:603–634
- Komen GJ, Cavaleri L, Donelan M, Hasselmann K, Hasselmann S, Janssen PAEM (1994) Dynamics and modelling of ocean waves. Cambridge University Press
- Kushnir Y, Cardone VJ, Greenwood JG, Cane MA (1997) The recent increase in North Atlantic wave heights. *J Clim* 10:2107–2113
- Lionello P, Sanna A (2005) Mediterranean wave climate variability and its links with NAO and Indian Monsoon. *Clim Dyn* 25: 611–623
- Lorenz EN (1956) Empirical orthogonal functions and statistical weather prediction. Technical report, statistical forecast project report 1, Dep Meteorol, MIT 49
- Magnusson A, Donelan M (2013) The Andrea wave characteristics of a measured North Sea rogue wave. *J Offshore Mech Arctic Eng* 135: 031108–1
- McCabe GJ, Clark MP, Serreze MC (2001) Trends in northern hemisphere surface cyclone frequency and intensity. *J Clim* 14:2763–2768
- Monahan AH, Fyfe JC, Ambaum MP, Stephenson DB, North GB (2009) Review empirical orthogonal functions: the medium is the message. *J Clim* 22:6501–6514. doi:10.1175/2009JCLI3062.1
- Mori N (2012) Freak waves under typhoon conditions. *J Geophys Res* 117:C00J07, 10.1029/2011JC007788
- Mori N, Janssen PAEM (2006) On kurtosis and occurrence probability of freak waves. *J Phys Oceanogr* 36(7):1471–1483
- Nesterov ES, Lukin AA (2012) Extreme waves in the North Atlantic. ISSN 1068–3739, *Russina Meteorol Hydrol*, 2012, No. 11, pp. 728–734. Allerton Press, Inc., 2012
- Ponce de León S, Guedes Soares C (2005) On the sheltering effect of islands in ocean wave models. *J Geophys Res* 110(C09020):1–17
- Ponce de León S, Guedes Soares C (2012) Distribution of winter wave spectral peaks in the seas around Norway. *Ocean Eng* 50:63–71
- Ponce de León S, Guedes Soares C (2014) Extreme wave parameters under North Atlantic extratropical cyclones. *Ocean Model* 81:78–88
- Queffeuilou P, Croize-Fillon D (2012) Global altimeter SWH data set. Version 9, April, Technical report, IFREMER
- Saha SS, Moorthi Pan HL, Wu X, Wang J, Nadiga S, Tripp P, Kistler R, Wooll J, Behringer D, Liu H, Stokes D, Grumbine R, Gayno G, Wang J, Hou YT, Chuang H, Juang HMH, Sela J, Iredell M, Treadon R, Kleist D, Van Dels P, Keyser D, Derber J, Ek M, Meng J, Wei H, Yang R, Lord S, van den Dool H, Kumar A, Wang W, Long C, Chelliah M, Xue Y, Huang B, Schemm JK, Ebisuzaki W, Lin R, Xie P, Chen M, Zhou S, Higgins W, Zou C, Liu Q, Chen Y, Han Y, Cucurull L, Reynolds RW, Rutledge G, Goldberg M (2010) The NCEP climate forecast system reanalysis bull amer. Meteorol Soc 91:1015–1057
- Sanders F, Gyakum JR (1980) Synoptic-dynamic climatology of the “bomb”. *Am Meteorol Soc* 108:1589–1606
- Serreze MC (2009) Northern hemisphere cyclone locations and characteristics from NCEP/NCAR reanalysis data. National snow and ice data center. Digital media, Boulder
- Tamura H, Waseda T, Miyazawa Y (2009) Freakish sea state and swell-windsea coupling: numerical study of the Suwa-Marui incident. *Geophys Res Lett* 36:L01607
- The earth observation handbook 2012—key tables, ESA (European Space Agency) and CEOS (Committee on Earth Observation Satellites), 41pp
- Verhoef A, Stoffelen A (2012) ASCAT wind product user manual Version 1.12. EUMETSAT/OSI SAF, 27 pp.

- Weisse R, von Storch H, Feser F (2005) Northeast Atlantic and North Sea storminess as simulated by a regional climate model during 1958–2001 and comparison with observations. *J Clim* 18:465–479
- Zhang HD, Cherneva Z, Guedes Soares C, Onorato M (2014) Modeling Extreme Wave Heights from Laboratory Experiments with the Nonlinear Schrödinger Equation. *Nat Hazards Earth Syst Sci* 14: 959–968